

PAPER-HILT: Personalized and Adaptive Privacy-Aware Early-Exit for Reinforcement Learning in Human-in-the-Loop Systems

MOJTABA TAHERISADR and SALMA ELMALAKI, University of California, Irvine, USA

Reinforcement Learning (RL) has increasingly become a preferred method over traditional rule-based systems in diverse human-in-the-loop (HITL) applications due to its adaptability to the dynamic nature of human interactions. However, integrating RL in such settings raises significant privacy concerns, as it might inadvertently expose sensitive user information. Addressing this, our paper focuses on developing PAPER-HILT, an innovative, adaptive RL strategy through exploiting an early-exit approach designed explicitly for privacy preservation in HITL environments. This approach dynamically adjusts the tradeoff between privacy protection and system utility, tailoring its operation to individual behavioral patterns and preferences. We mainly highlight the challenge of dealing with the variable and evolving nature of human behavior, which renders static privacy models ineffective. PAPER-HILT's effectiveness is evaluated through its application in two distinct contexts: Smart Home environments and Virtual Reality (VR) Smart Classrooms. The empirical results demonstrate PAPER-HILT's capability to provide a personalized equilibrium between user privacy and application utility, adapting effectively to individual user needs and preferences. On average for both experiments, utility (performance) drops by 24%, and privacy (state prediction) improves by 31%.

CCS Concepts: • **Human-centered computing**; • **Security and privacy** → **Privacy protections**; • **Computing methodologies** → **Reinforcement learning**;

Additional Key Words and Phrases: Reinforcement learning, early-exit, privacy, human-in-the-loop

1 INTRODUCTION

The rapid evolution of sensor networks and mobile computing has given us unprecedented capabilities to observe human behavior and their interaction with their environment, paving the way for developing human-aware Internet of Things (IoT) applications [12]. This synergy between human behavior and technology is revolutionizing the design of IoT applications, leading to the emergence of Human-in-the-Loop (HITL) IoT systems [7]. By continually sensing and adapting to both the environment and human inputs, these systems offer a novel paradigm in IoT, promising highly personalized user experiences in these advanced technologies.

However, this intimate integration of human behavior with IoT systems introduces significant privacy challenges. The diversity in human behavior patterns, routines, and preferences, which greatly influence the data generated, can lead to varied levels of privacy vulnerabilities. In particular, this behavioral diversity leads to distinct privacy implications, as certain individuals' behavior may inadvertently leak sensitive information in some cases more than in others [6, 51]. Accordingly, when designing AI algorithms in HITL IoT systems, it is crucial to recognize that privacy considerations are not static but can dynamically evolve due to shifts in human behavior. Recognizing these nuances and tailoring privacy mitigation algorithms accordingly becomes essential for ensuring the responsible utilization of HITL IoT technologies. This approach to privacy mitigation acknowledges that privacy is not a one-size-fits-all concept [4, 27].

In addressing these challenges, this paper focuses on mitigating privacy leaks in machine learning-based HITL IoT systems. We explore the use of privacy-aware Deep Reinforcement Learning (DRL), an approach that has shown promise in adapting to human intentions and responses [22, 47]. Our focus on RL stems from its adoption in methods such as Multisample RL and adaptive scaling RL (ADAS-RL) that can accommodate variations in both inter- and intra-human variability in behaviors, adapting to a wide range of automated actions [1, 13]. Furthermore, recent research has highlighted the potential of RL models to address concerns related to equity, fairness, risk sensitivity, safety, and human diversity [11, 13, 16, 23, 58].

DRL's ability to personalize IoT systems for individual experiences is well-documented, yet it also raises privacy concerns due to its potential to access private human states [42]. This issue is particularly pertinent in domains like healthcare, finance, and autonomous vehicles, where the continuous use of sensitive user data poses significant privacy concerns [24]. Therefore, balancing the need for personalized HITL IoT experiences with protecting individual privacy is a critical challenge.

Previous research has explored privacy vulnerabilities in learning-based RL systems, often focusing on the privacy-utility tradeoff. However, the unique context of HITL IoT systems presents distinct challenges. Recognizing the inherent variability

Authors' address: Mojtaba Taherisadr, taherisa@uci.edu; Salma Elmalaki, salma.elmalaki@uci.edu, University of California, Irvine, Irvine, California, USA, 92617.

2024. Manuscript submitted to ACM

among human subjects, we propose PAPER-HILT, an adaptive personalized DRL approach that leverages an early-exit strategy. This approach aims to tailor the privacy-utility tradeoff to individual variability in HITL IoT.

2 RELATED WORK AND PAPER CONTRIBUTION

Privacy concerns have persisted for many years [46], prompting extensive research to address privacy breaches and their mitigation through various strategies. Hong et al. [25] addressed the imperative of balancing privacy and model performance through differentially private learning. Their work introduces dynamic policies, including adjustments to model parameters. These dynamic techniques enhance the performance of the models within privacy constraints. Game-theoretical methods have been employed to create an objective function that maximizes utility while minimizing privacy vulnerabilities [28]. Additionally, data encryption has been proposed as a defense against side-channel attacks on communication links between edge and cloud services [39]. Zhang et al. [57] tackle training data privacy in machine learning, shifting focus to attribute privacy and concealing sensitive dataset properties during analysis. They propose definitions and efficient mechanisms for safeguarding specific dataset properties and distribution parameters, laying the foundation for addressing attribute privacy in preserving global properties during analysis. Patel et al. [45] address information leakage in model explanations for algorithmic transparency. They introduce differentially private mechanisms, balancing transparency and data privacy in machine learning.

Our emphasis on using reinforcement learning (RL) methods is driven by two critical attributes:

- **Computational Complexity and Scalability:** RL offers computational scalability advantages compared to other techniques, especially game-theoretic approaches. Many game-theoretic methods for sequential decision-making are recognized as computationally infeasible [18].
- **Generalizability:** RL possesses a unique capacity to directly model the consequences of decisions, leverage temporal feedback during the learning process, and enhance decision-making policy performance across a broad spectrum of systems. This attribute is particularly valuable for Human-in-the-Loop (HITL) systems.

2.1 Related Work

2.1.1 Privacy-preserving RL. Several facets of privacy-preserving RL challenges have been explored and addressed, including online learning with bandit feedback [35], linear contextual bandits [19], and deep reinforcement learning (DRL) [43]. In the tabular setting, Garcelon et al. [20] introduced an algorithm that ensures both regret minimization and privacy preservation. In continuous state scenarios, Wang et al. [55] devised a Q-learning variant capable of discovering a policy that adheres to differential privacy constraints while optimizing the reward function. Erdemir et al. [15] studied the trade-off between privacy and utility (PUT) in this context, noting that existing approaches often overlook temporal correlations in time-series data. They proposed sharing a distorted version of the user data sequence to mitigate privacy risks. Their approach quantifies privacy risk through mutual information assessment and employs asynchronous actor-critic deep reinforcement learning (RL) to minimize history-dependent mutual information. adaPARL [51] examined the privacy leaks inherent in sequential decision-making setups for HITL IoT, where interactions with humans introduce variability in behavior and preferences over time. It introduces an adaptive privacy-aware algorithm for such systems, which adjusts to varying human behaviors. adaPARL is designed based on Q-learning and is typically used for discrete state and action spaces. The drawback of limited state space encourages exploring more advanced RL algorithms.

2.1.2 Early Exit in HITL IoT. The concept of Early Exit (EE) was initially proposed by Teerapittayanon et al. [52] to eliminate the necessity of reducing the size of deep neural network (DNN) models. This is achieved by introducing early exits within the DNN architecture, which enables the termination of execution as soon as a desired confidence level is reached for a given input sample. In practical terms, certain samples in test datasets and real-world scenarios can be readily processed by a DNN model. In contrast, others might pose challenges, depending on the specific machine learning models employed. Consequently, EE optimizes the inference process for straightforward samples by reducing the number of transformation layers involved, thus reducing overall inference time and computational costs [37]. Some work in the literature examined the effects of EE mechanism in IoT and federated learning scenarios, aiming to enhance the robustness of training and inference against privacy attacks, such as Membership Inference Attacks (MIAs) [56]. EE-equipped models in dynamic neural networks adjust their computation path for each sample based on its complexity. The study employs threshold and logistic regression attacks to measure privacy, revealing that EE techniques improve privacy preservation. Through experiments, they determined that models lacking early exits are more

susceptible to MIAs. The vulnerability of Convolutional Neural Network (CNN), AlexNet, and ResNet18 models to these attacks is assessed in both centralized and federated learning settings. The findings highlight the potential of dynamic architectures in enhancing privacy, underscoring the need for further exploration and design in this model category [56].

While EE strategies have been extensively explored in the context of DNN, their application in RL settings offers a novel perspective on improving the efficiency of learning algorithms. The concept of terminating an episode prematurely, based on intermediate observations or partial trajectories, holds promise in accelerating convergence and optimizing resource utilization. RAPID-RL [33] introduces a novel approach to enhance deep RL. RAPID-RL framework enhances a standard *DQN* with multiple exit branches, enabling the rapid inference of most input states and leading to quicker processing and reduced compute operations. Additionally, they present a sequential training method for these branches, ensuring optimal performance for each while circumventing performance interdependence and creating a unified joint *DQN* adhering to power constraints. In this paper, we exploit EE for *DQN* and explore its efficiency as a privacy mitigation technique in HITL IoT systems with human variability.

2.2 Paper Contribution

Our contributions can be summarized as follows.

- (1) **PAPER-HILT:** We propose an algorithm for personalized privacy-aware HITL systems with human behavior variability. This algorithm is based on DRL with EE and is tailored for sequential decision-making systems.
- (2) **Personalization:** We offer the capability to personalize the tradeoff between privacy mitigation and the application’s utility. It is designed to adaptively mitigate privacy leaks based on the variability in human behavior.
- (3) **Versatility and adaptability:** We introduce general design parameters within our proposed algorithm that can be adjusted to suit the requirements of various application domains.
- (3) **Simulation and real-world applications:** We implement our proposed algorithm in two HITL systems: a simulated smart home environment and a real-world smart classroom with VR technology.

The paper is organized as follows: Section 3 reviews the deep reinforcement learning for the Human-in-the-Loop systems. Then, we structure the threat model for the HITL IoT technologies in Section 4. The paper’s subsequent sections focus on the PAPER-HILT algorithm and then evaluate the proposed PAPER-HILT algorithm on two different applications.

3 DEEP REINFORCEMENT LEARNING (*DQN*) FOR HUMAN-IN-THE-LOOP APPLICATIONS

Deep Q-Networks (*DQN*), a reinforcement learning paradigm, integrates deep neural networks with Q-learning, operating within the framework of Markov Decision Processes (MDP). The crux of *DQN* lies in estimating the action-value function $Q(s, a)$, which encapsulates the expected rewards for actions within specific states. This function is typically represented by a neural network with state inputs and estimated action values as outputs. At each discrete time step t , the *DQN* agent employs an ϵ -greedy strategy for action selection. It updates the Q-function based on observed states, rewards, and the next state using an update rule:

$$Q(s_t, a_t) \leftarrow Q(s_t, a_t) + \alpha(r_{t+1} + \gamma \max_a Q(s_{t+1}, a) - Q(s_t, a_t)), \quad (1)$$

where α is the learning rate, γ is the discount factor, and $\max_a Q(s_{t+1}, a)$ is the estimated maximum action-value in the next state s_{t+1} .

DQN aims to learn a policy $\pi(s, t)$ that maximizes the cumulative reward over time in a given environment. It combines Q-learning with deep learning, allowing the agent to handle high-dimensional observations and non-linear function approximations.

DQN can model the dynamic interplay between environments and human interaction. Through interaction with the HITL environment, the *DQN* agent continually updates these Q-value estimates, guided by the reward signals originating from humans. These rewards, whether stemming from explicit annotations or implicit cues, enable the agent to learn between favorable and undesirable actions, ultimately reinforcing the learning of optimal policy $\pi(s, a)$ that shape the HITL adaptation [10].

In this ecosystem, humans are more than mere bystanders; they are active contributors whose feedback shapes the reward landscape for the *DQN* agent. This feedback, manifested in various forms like explicit annotations or subtle sensory cues, is categorized as positive (indicating “good” human experience) or negative indicating “bad” human experience). The integration of these human-originated rewards is pivotal in steering the RL agent towards learning optimal policies. These policies, in turn, dictate the adaptive actions executed within IoT systems, aligning technological innovation with human-centric values.

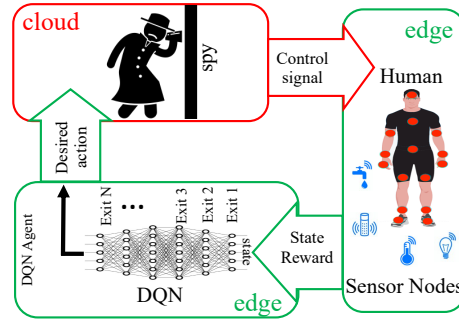


Fig. 1. Threat Model for HITL IoT application.

4 THREAT MODEL IN HITL IOT TECHNOLOGIES

Recent advancements in edge devices' power and memory capabilities have enabled the execution of relatively resource-intensive computations at the edge. Consequently, it can be assumed that the edge layer can perform demanding data processing tasks, including raw data processing and the execution of RL algorithms. Moreover, synchronizing numerous applications, particularly in pervasive environments, necessitates a central decision-making server operating at a cloud-based level. As a result, the edge layer does not directly transmit control actions to the environment. Still, it must first share them with the cloud to address various constraints it may need to enforce, such as synchronizing multiple applications. This edge-cloud computing model represents a typical architecture for numerous pervasive and ubiquitous applications [5, 44, 49].

The proposed threat model can be summarized as follows:

- An application operating under the HITL paradigm collects information from the environment and human interactions through multiple sensors on edge devices.
- A *DQN* agent runs on the edge to infer the state of the human and the environment and recommends adaptive actions based on human preferences and behavior.
- Only the recommended action generated by the *DQN* agent is communicated to a cloud-based server; in particular, the inferred states of the environment or the human are not shared with the cloud. The Edge is considered a trusted entity.
- The cloud selects the appropriate control signals, which may be based on other enforced constraints, and sends them to actuator nodes (edge devices) for adaptation in the environment.

Therefore, based on this threat model, our attack vector is as follows:

- An eavesdropper is positioned within the cloud and cannot access edge devices (sensors or actuators) or the communication channel between the edge and the cloud.
- The eavesdropper has access to the time-series data of the desired recommended actions within the cloud.
- The eavesdropper can employ any machine learning model leveraging this time-series data.
- The eavesdropper possesses prior knowledge of the application domain.

In this attack vector, even if the communication channel between the edge and the cloud is secured (e.g., through encryption), the cloud is still required to decrypt the transmitted packet, which contains the desired action, to select the control signals to be sent back to the edge actuators for pervasive applications. Consequently, the eavesdropper can observe and record the time-series data of the desired actions of this application. Figure 1 illustrates the threat model and attack vector. Our objective in this study is to provide a guarantee that limits the ability of an eavesdropper to infer the private state, even with unlimited computational power and complete knowledge of the application domain.

5 PAPER-HILT ALGORITHM

PAPER-HILT algorithm addresses the challenge of balancing the privacy-utility trade-off in HITL systems using *DQN* models. Our approach entails training *DQN* to decide the optimal layer within the network at which an exit should be taken based on the two objectives of utility and privacy. Specifically, the algorithm employs two criteria for identifying network exit points that maximize utility while ensuring privacy protection. To achieve this, PAPER-HILT evaluates each early exit branch's ability to provide a reasonable trade-off between utility and privacy. This distinctive methodology offers a personalized and adaptive

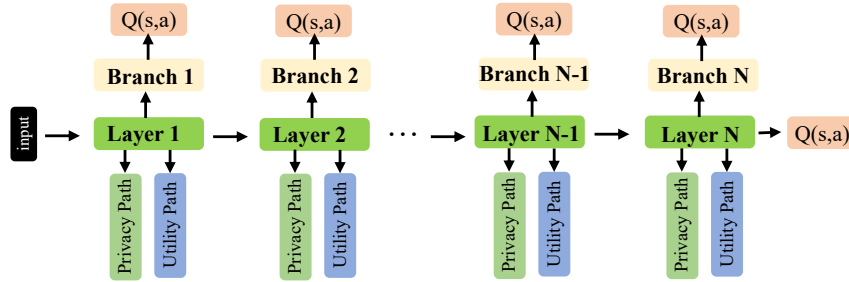


Fig. 2. Structure of the PAPER-HILT algorithm. Each layer is followed by an exit branch and two confidence paths associated with the utility and privacy. Branches and confidence paths are trained independently.

mechanism to determine exit points based on human behavior variability, ultimately allowing for more personalized privacy-aware decision-making during inference. A pictorial figure for PAPER-HILT is shown in Figure 2. In particular, the DQN is designed with early exit (EE) at every layer, providing a particular utility and privacy budget. The training process consists of two phases. In the first phase (**PHASE 1**), we train the DQN with all of the EE branches. Then, in the second phase (**PHASE 2**), we fine-tune the branches based on the privacy and utility budgets. In the following, we will provide a detailed explanation of the training phases.

5.1 Privacy Leak Metric

We draw upon the information theory literature and employ mutual information (MI) to quantify the degree of correlation (or dependence) between two random variables. In our specific context, we utilize MI to gauge how effectively an eavesdropper can deduce a system state from observed actions. MI establishes a theoretical limit on the inferential capability of any learning algorithm. Generally, the lower the MI between the state and action, the less accurate any inference algorithm can be. To illustrate the extreme case, no algorithm can infer the state from the observed actions when MI is zero. Therefore, we regard the MI measure $\mathcal{I}_\pi(a_t; s_t)$ for a given policy $\pi(s, a)$ as a quantifiable constraint on the capacity to extract maximum information about s_t by observing a_t . Specifically, the information disclosed to the eavesdropper is bounded by $\mathcal{I}_\pi(a_t; s_t)$. We will exploit this metric to determine the privacy leak at each exit, as shown in Figure 2.

5.2 PAPER-HILT training

Training PAPER-HILT entails the following design choices: (1) the placement of the EE branches in DQN , (2) the architecture of these EE branches, (3) the criteria that determine when a branch should be taken to exit, and (4) the training strategy applied to these criteria for branches. We divide our training for PAPER-HILT into two phases, as explained below.

5.2.1 PHASE 1: Train DQN with EE. The process of training a Deep Q-Network (DQN) to learn the optimal policy, denoted as $\pi(s, a)$, is a dynamic procedure that requires interaction with the environment. This interaction is through taking actions generated by the policy of an online Q-network. These actions and states are accumulated within an experience replay buffer. This buffer serves as a reservoir of past experiences. Periodically, at predefined intervals during the training phase, a batch of transitions is randomly sampled from this experience replay. These sampled transitions are subsequently evaluated using a separate entity known as the target Q-network, which plays a crucial role in stabilizing the learning process. The target Q-network helps approximate the expected future rewards, guiding the DQN toward the optimal policy. The parameter updates made in the online Q-network are based on the calculated loss, which varies depending on the specific application or task. This loss reflects the disparity between the Q-values estimated by the online Q-network and the target Q-network. Consequently, this entire training process is designed to optimize the performance of DQN within application environments, and the success of the model relies on the iterative refinement of these interactions and updates.

Our first training phase (**PHASE 1**) is to train DQN with EE. We exploit the recent work in the literature that proposes a “sequential training” approach [33]. It starts with a single-layer Q-network and gradually expands by introducing and training a new layer with a new exit one at a time while keeping the parameters of previously trained layers and exit branches fixed. As

a result, the previously trained layers and branches remain unaffected when a new layer and branch are introduced. Figure 3 illustrates *DQN* with EE using sequential training¹.

5.2.2 PHASE 2: Train for privacy-utility tradeoff. The resulting *DQN* from PHASE 1 contains EE branches, each individually optimized to deliver peak performance at this exit per a predefined application utility. However, as motivated earlier, we want to train PAPER-HILT to deliver a privacy-utility tradeoff. This tradeoff should account for the dynamic nature of the environment and the varying behavior of humans. Accordingly, as seen in Figure 2, each EE branch maintains a *confidence labels* on the utility and privacy at this branch (generated by the privacy and utility paths). Hence, based on a particular privacy-utility tradeoff, a particular EE branch will be chosen to exit.

The intuition is that we want to give each EE branch two labels: a utility label and a privacy label. Each label can take a value of “1” or “0” to indicate if a particular EE satisfies a particular utility or privacy budget (given a label “1”). These labels will determine which EE branches are available to exit based on a particular utility and privacy budget.

To achieve this, we further augment the trained *DQN* with two other paths, utility path, and privacy path, at each exit that will output these labels. We train these two paths to learn these labels based on two parameters: ‘*u*’ representing the *utility budget* and ‘*p*’ representing the *privacy budget*. Lower values of ‘*u*’ and higher values of ‘*p*’ prioritize privacy while potentially sacrificing utility. Conversely, higher ‘*u*’ and lower ‘*p*’ values favor utility-centric learning at the potential expense of privacy leaks. Thus, depending on the specific application requirements and the variation of human behavior patterns, the tradeoff between ‘*u*’ and ‘*p*’ governs the exit selection in the *DQN*.

Utility Confidence Label (UCL) Training: For the utility confidence label training, we follow the [33]. During the interaction of the trained model from **PHASE 1** with the environment, we create a utility replay buffer containing the state, action, and utility labels. We randomly choose one of the actions determined by the branches. Monitoring the max of the q-values of each branch (Q_{imax}), we create labels for all branches for the replay buffer, where Q_{imax} is the maximum of all of the branches.

$$UCL_i(s, a) = \begin{cases} 1, & \text{if } Q_{imax}(s, a) > u \times Q_{max}(s, a) \\ 0, & \text{otherwise,} \end{cases} \quad (2)$$

where parameter $u \in (0, 1]$ is the utility budget that determines the amount of the utility that we want to preserve.

Privacy Confidence Label (PCL) Training. Similarly, to train *PCL*, we let the trained *DQN* from **PHASE 1** interact with the environment. During this interaction, the input to the *DQN* is the current environment state with the human-in-the-loop s , and then each EE will output one action a . As explained in Section 5.1, we use MI as a metric to measure the privacy leak. We use $I_i(s, a)$ to represent the MI of branch i ². At the end of every n_{th} interaction with the environment, the min of MI of all branches for the past n interactions is calculated as $I_{max}(s, a) = \max(I_i(s, a))$. The *PCL* is then determined as,

$$PCL_i(s, a) = \begin{cases} 1, & \text{if } I_i(s, a) < p \times I_{max}(s, a) \\ 0, & \text{otherwise,} \end{cases} \quad (3)$$

here, the *PCL* of branch i is set to 1 if the $I_i(s)$ is smaller than the I_{max} multiplied by a constant $p \in (0, 1]$; otherwise, it is set to 0. This parameter p is the *privacy budget* as described earlier. A higher p prioritizes high privacy, while a lower p results in more exits at the cost of privacy.

Accordingly, to train this label, PAPER-HILT augments the trained Q-network with a branch called a privacy path that is going to output this label at every exit³. Hence, an experience replay buffer is created that contains the state, action, and all the *PCL* from all the branches. Since we have different actions from each EE branch, the action (a) chosen for a given input state (s) is selected randomly from the actions predicted by all the EE branches (a_i) to prevent bias towards a specific branch.

Figure 4 shows this process of maintaining privacy and utility reply buffers for every *DQN* interaction with the environment. By adopting this confidence-label training framework for utility and privacy, we allow for EE that considers privacy preservation and utility maximization based on a particular privacy budget p and a utility budget u . The two training phases are described in

¹We used a branch layer of two fully connected layers and an output layer which generates the q values.

²As MI can only be determined through a time series, we update the privacy replay buffer for every n interaction.

³We used a branch of a fully connected layer with a binary cross-entropy (BCE) loss that creates a binary output as the confidence outcome.

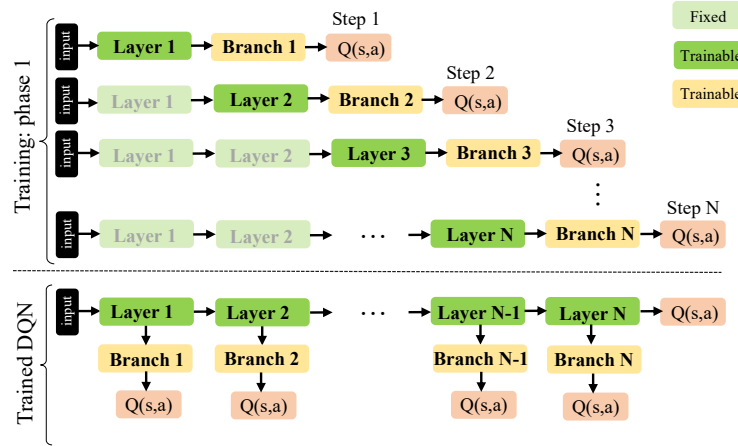


Fig. 3. Phase 1 of the training flow of the PAPER-HILT algorithm. An exit branch follows each layer. The layer and associated branch are trained in each step, and the next layer and its branch are added in the following step. Training of the new layer and its branch happens while the parameters of the previous layers and branches are frozen.

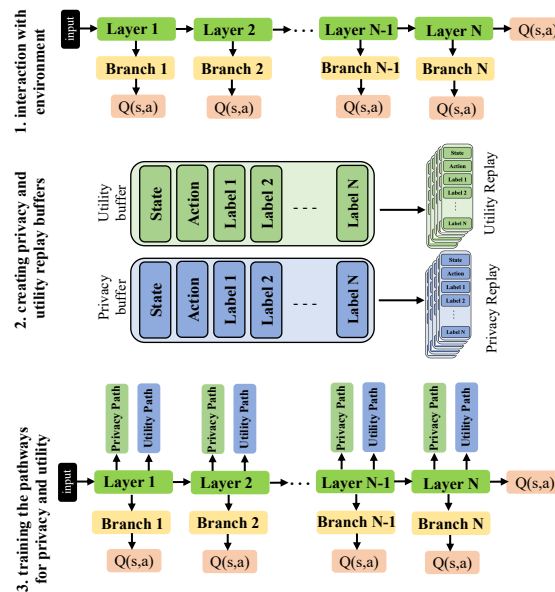


Fig. 4. Phase 2 of the training: Privacy and utility confidence path training for each exit branch of the DQN . The network has two separate buffers. The privacy buffer contains the action, state, and privacy labels for all branches. The utility buffer includes the action, state, and utility labels of the branches.

the Algorithms 1 and depicted in Figure 4. In particular, at the end of this training, each EE branch will give three outputs, $Q(s, a)$ from PHASE 1 training, and the two labels (UCL and PCL).

5.3 PAPER-HILT Inference

Once the training is complete, the trained DQN with the confidence paths is deployed to guide the model's decision-making process. The algorithm utilizes confidence branches at each decision point to make informed choices regarding the optimal exit. The EE is selected to align with the specified utility (u) and privacy (p) budgets as shown in Algorithm 2.

Algorithm 1: Phase 1 & 2 of the *DQN* training**Input:**

Environment \mathcal{E} ,
 Number of layers n ,
 Utility budget u ,
 Privacy budget p .

Output:

Trained Q-network Q with utility and privacy confidence labels.

PHASE 1:

Initialize Q with random weights. **for** $layer \leftarrow 1$ **to** n **do**

 Add branch for layer $layer$. **while** *Training* **do**

 Sample a transition tuple (s, a, r, s') from \mathcal{E} ;

 Compute the Q-value target;

 Compute the Q-value estimate; Compute the loss $\mathcal{L} = \text{mean squared error}(Q_{\text{target}}, Q_{\text{estimate}})$;

 Update the parameters using gradient descent.

 Freeze the parameters of layer $layer$ and its branch. Add layer $layer + 1$ to Q .

PHASE 2:

Input:

Trained n layered Q-network Q ,
 Utility budget u ,
 Privacy budget p .

Interact with the environment;

Create privacy and utility buffers (Choose a_i randomly from the branches);

Utility buffer (s, a, UCL) for utility training;

Privacy buffer (s, a, PCL) for privacy training;

Augment Q with branches for the privacy and utility confidence paths.

while *Training* **do**

 Sample (s, a, UCL) from Utility buffer;

 Sample (s, a, PCL) from Privacy buffer;

 Train privacy and utility confidence paths;

 Update the parameters of the confidence paths.

Algorithm 2: Inference using a Trained *DQN***Input:**

State: s ;

Trained *DQN* with n branches trained for a particular privacy p and utility u budgets: Q ;

Output:

Branches satisfy privacy p and utility u budgets;

Take the current state s as input

for *Each branch* i **in** Q **do**

 Get the action a_i for branch i based on current s ;

 Retrieve the confidence scores for privacy and utility as PCL_i and UCL_i ;

if $PCL_i = 1$ **then**

 Branch i is satisfactory for the privacy budget p ;

if $UCL_i = 1$ **then**

 Branch i is satisfactory for the utility budget u ;

5.4 Incooperating Human Variability

As mentioned earlier, human behavior is not fixed, and hence, the labels used (*PCL* and *UCL*) to train the confidence path can change over time. Hence, after the trained *DQN* is deployed, PAPER-HILT accumulates a repository of interactions with the environment, which contains selected actions, state observations, and corresponding rewards associated with the chosen exit branch. This repository will be used to monitor the variations in MI. If these variations drop below a predetermined threshold (as an indication of the change in the human behavior), PAPER-HILT initiates a training phase, wherein the *DQN* is retrained to adapt to the evolving environment, effectively accommodating variations in user behavior or environmental conditions. We set

Algorithm 3: Inference and human variability-aware *DQN* retraining**Input:**

State s ;
 Trained *DQN* with n branches with a particular privacy p and utility u budgets: Q ;
 Replay buffer size: \mathcal{B} ;
 Human variability threshold: $I_{\text{threshold}} = v \times I_{\text{max}}$, where $v \in [0, 1]$;

Output:

Retrained *DQN* with n branches Q' .

Initialize a replay buffer \mathcal{B} ;

while *Inference with Q* **do**

 Update the replay buffer \mathcal{B} ;
 Monitor I_{current} of the selected exit branch;

if $I_{\text{current}} < I_{\text{threshold}}$ **then**

 Train Q' using the data in \mathcal{B} ;

$Q = Q'$

 Reset \mathcal{B} ;

this threshold as a percentage of the max of the MI (I_{max} at the point the agent converges to a specific action that maximizes the reward that we reach during **Phase 1** of the training). $I_{\text{threshold}} = v \times I_{\text{max}}$, where $v \in [0, 1]$. This continuous training through updating the *DQN* whenever the human behavior or environment changes is described in Algorithm 3.

6 APPLICATION 1 - HOUSE MODEL

Recent research in the field of smart heating, ventilation, and air conditioning systems (HVAC) with human-in-the-loop aims to enhance human satisfaction [11, 29]. Accordingly, it is essential to incorporate human conditions and preferences into the decision-making process when determining the HVAC setpoint. For instance, the human body temperature naturally decreases during sleep [3], while it rises during physical exercise [34], and in response to stress and anxiety [41]. To monitor human conditions such as sleep patterns and physical activity, IoT edge devices can be used [40, 48]. These devices can play a crucial role in gathering relevant data. However, it's worth noting that while the primary objective of this section is to assess the trade-off between privacy and utility offered by our model, we will first provide an overview of the IoT environment design and the DRL agent used for this specific application.

6.1 Human-in-the-Loop IoT System Design

In our study, we simulated a thermodynamic model representing residential houses. This model considers various factors, such as the house's architectural design, the number of windows, the roof's pitch angle, and the insulation material employed. The heating system in the house is facilitated by a heater, which releases air at a temperature of 50°C , while cooling is achieved through a cooler that emits air at 10°C . To regulate the indoor temperature, a thermostat is employed, which permits a deviation of up to 2°C both above and below the desired set-point. This setpoint temperature is managed by an external controller running PAPER-HILT [36].

In our approach, we represent humans as thermal sources, with heat generation influenced by both the average exhale breath temperature (*EBT*) and the respiratory minute volume (*RMV*) [11]. The *RMV* is determined by the breathing frequency (f) and the volume of gas exchanged during each breathing cycle, which varies significantly based on the level of human activity [9].

We model the behavior of three distinct human subjects in three homes by manipulating their *RMV* and metabolic rate. Our simulation encompasses six activity categories, including five related to in-home activities and a state labeled as "not at home." These categories include sleeping, relaxing, watching TV, cooking, and exercising. Each human is characterized by unique and diverse lifestyle patterns. Human H_1 adheres to a structured routine that repeats weekly, displaying limited randomness. In contrast, H_3 exhibits a highly irregular lifestyle with activities that lack a specific daily or weekly pattern, featuring numerous unexpected changes. H_2 falls in between, displaying a moderate level of randomness compared to H_1 and H_3 . Figure 5 provides a visual representation of the behavioral pattern of H_1 , H_2 , and H_3 showcasing alternating engagement in six primary activities, including sleeping, not at home, watching TV, cooking, exercise, and relaxation.

To introduce variability into our simulation, we randomly assign different activities within the same time slots to create three diverse daily human behaviors. It is important to note that we do not account for factors such as age, sex, or time of day in our

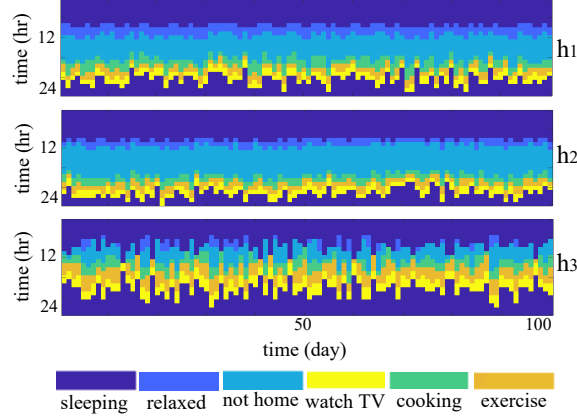


Fig. 5. Human activity profile for three humans.

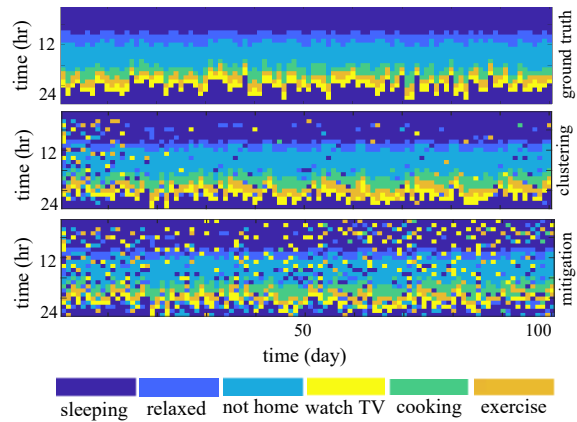


Fig. 6. Activity pattern of the house model. Top: ground truth of the activity patterns of human H_1 . Middle: clustering result as seen by the eavesdropper. Bottom: clustering result after applying mitigation with PAPER-HILT at $p = 0.7$ and $u = 0.75$.

model. We have expanded the thermal house model provided by Mathworks to incorporate a cooling system and our human simulation [36]⁴. Each simulation step corresponds to one hour and every 24 steps is one day.

6.2 DRL Design

We have developed a DRL framework, which is elaborated upon below, to personalize the HVAC setpoint according to human activity and the desired level of thermal comfort.

6.2.1 State, Action, and Reward. State space \mathcal{S} : For every possible combination of six unique human activities and the indoor temperature of the house, our state space \mathcal{S} is defined as $\mathcal{S} = \{(act, temp) : act \in [1, 6] \text{ and } temp \in [60, 80]\}$. Here, act represents the current human activity, and $temp$ represents the current temperature inside the house, a continuous value. Action Space \mathcal{A} : we consider discrete values within the temperature range of $[60, 80]$, including heating and cooling options. Reward \mathcal{R} : We used Prediction Mean Vote (PMV) as a means to gauge human thermal comfort [17]. The PMV scale spans -3 (indicating very cold) to 3 (indicating very hot). According to the ISO standard ASHRAE 55 [2], maintaining a PMV within $[-0.5, 0.5]$ for indoor spaces is recommended to ensure thermal comfort. Estimating the PMV score relies on clothing insulation, metabolic rate, air vapor pressure, temperature, and mean radiant temperature [17]. Hence, PMV values falling within $[-0.5, 0.5]$ yield positive rewards, while PMV values indicating discomfort result in negative rewards. In practical applications, PMV can be estimated using edge devices, such as black globe thermometers [8].

⁴While more complex simulators like EnergyPlus exist for comprehensive assessments of energy consumption and electrical loads in smart houses and buildings [21], we have opted for a simplified thermal house model to evaluate PAPER-HILT.

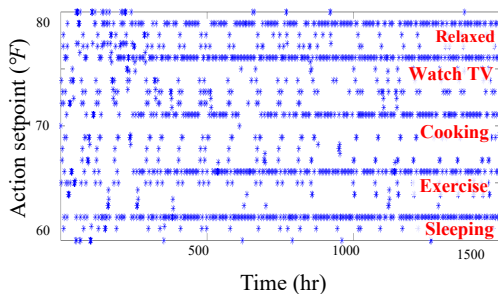


Fig. 7. Action convergence of human H_1 using DQN .

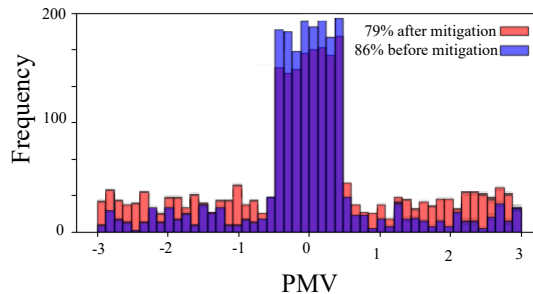


Fig. 8. PMV before and after applying PAPER-HILT mitigation using utility budget $u = 0.75$ and privacy budget $p = 0.7$ for H_1 .

6.3 Evaluation

Our evaluation strategy starts by first showing PAPER-HILT’s ability to adapt to different human behavior patterns by choosing different EE for each human to achieve a utility budget u (Section 6.3.1). Afterward, we assess the privacy leak resulting from this personalization based on our threat model (Section 6.3.2). Then, we show the effect of using PAPER-HILT with PCL and UCL at a particular privacy p and utility u budgets on privacy leak mitigation (Section 6.3.3). Finally, we analyze the tradeoff of choosing p and u in this application (Section 6.3.4). Our results show that using PAPER-HILT, we were able to provide *personalized* privacy leak mitigation by improving privacy protection.

6.3.1 PAPER-HILT Adaptation. PAPER-HILT’s architectural design involves considerations that can be viewed as design hyperparameters. These include determining the location of exit branches and defining the structure of the exit branch. We start by designing a DQN model without exit branches to analyze the performance relationships with the base network architecture. First, we design DQN models with varying sizes from 1 to 10 and measure the PMV percentage in the comfortable range ($[-0.5, +0.5]$) for different layer depths per human as the metric for the utility performance of the network. As the agent interacts with the simulated environment to maximize the PMV in the comfortable range, DQN s with varying depths learn to converge to specific actions. Figure 7 demonstrates the convergence of actions as the training progresses for a DQN of 6 layers, revealing how the DQN model converges to specific actions for H_1 .

Our analysis demonstrates that for H_1 , the network with a depth of 6 layers outperformed network depths, while for H_2 and H_3 , the optimal number of layers were 8 and 3, respectively. Outperformed depths of layers are in the range 1 to 10, which indicates that the base model of depths 10 is a proper choice for PAPER-HILT architecture design for this application.

We designed a DQN of 10 fully connected layers with a branch composed of 2 fully connected layers for each base layer. The employed loss function is the mean square error (MSE) of the online and target Q networks, which utilize a replay buffer containing action, state, and reward information for updating the network’s parameters. A batch size of 16 (1 sample per hour) was used to train the model, which means it takes 16 hours to have enough samples in the replay to update the model parameters. We examined the impact of using base DQN s (without branches) with varying layers on the system performance in this setup. Subsequently, we started **PHASE 1** in PAPER-HILT, which has “sequential training” with up to 10 layers. We trained three independent DQN s for the three humans. We measured the MI and PMV for all exit branches to assess the relationship between utility performance and information leakage. Figure 9 depicts the MI and PMV for H_1 for all exit branches. The first row of Figure 9 shows the MI between the chosen action for that exit branch and the input state s . The second row plots the histogram of the PMV values for each exit branch as they interact with the environment, where the percentage value indicates the percentage of the PMV values in the comfortable range of $[-0.5, +0.5]$. Figure 9 shows that both MI and PMV percentages were highest at branch 6, indicating that higher utility performance reveals more private information about the user.

6.3.2 Privacy Leak. We assess this application’s potential risk of private information leakage, assuming that an eavesdropper can monitor the DRL agent’s actions. This scenario is plausible when we consider a smart thermostat system utilizing a cloud-based service, such as NEST [54], along with a covert spyware eavesdropper situated within the cloud infrastructure as discussed in our threat model in Section 4.

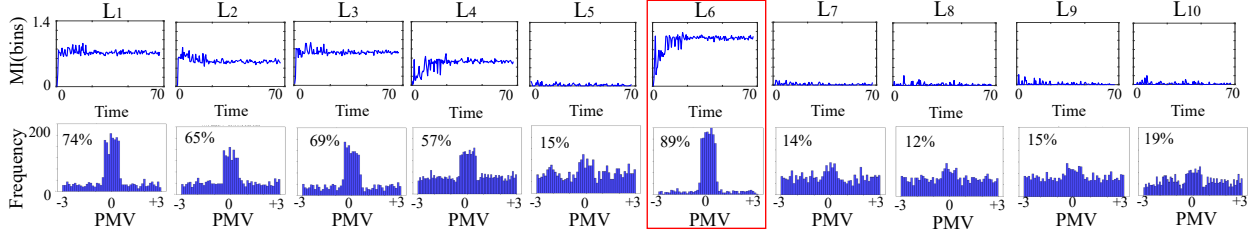


Fig. 9. PMV and corresponding MI at every branch for human H_1 . Top: mutual information between the current state and the chosen action in the associated exit layer. Bottom: PMV histogram for the associated exit with the percentage of the PMV values in the comfortable range $([-0.5, +0.5])$. Mutual information and PMV percentage in the comfortable range occurs at the layer 4 exit branch.

u	u = 0.85									
L	L ₁	L ₂	L ₃	L ₄	L ₅	L ₆	L ₇	L ₈	L ₉	L ₁₀
H ₁						✓				
H ₂								✓		
H ₃			✓							

Table 1. Permitted exit branches for the utility budget $u = 0.85$ for all human subjects.

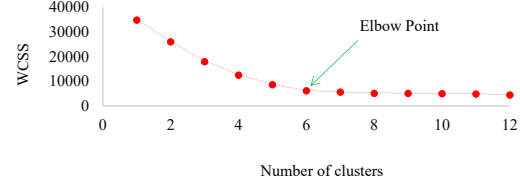


Fig. 10. WCSS vs. the number of clusters for human H_1 .

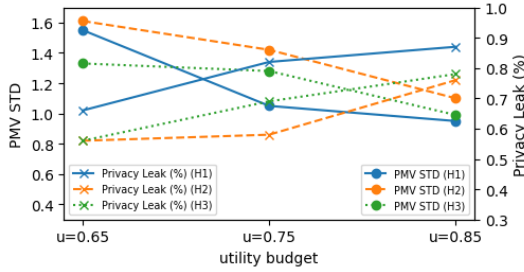
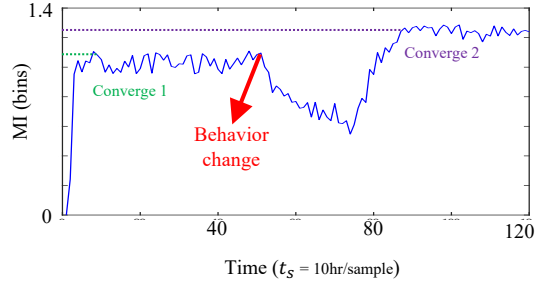
Given that the eavesdropper possesses no prior knowledge about human behavior within the household, they might use unsupervised learning techniques to deduce concealed patterns. For instance, by implementing a simple clustering algorithm, such as K -means, the eavesdropper can reveal sensitive information such as occupancy and sleeping schedules. Since the eavesdropper lacks prior knowledge regarding human activity, the optimal number of clusters remains unknown. Consequently, a possible method for the eavesdropper is to utilize the elbow point technique to find the most appropriate number of clusters. Utilizing the clustering on the actions shared with the cloud engine from the branch that maximizes the utility (in this case exit branch 6 for human H_1), an eavesdropper can plot the WCSS (Within-Cluster Sum of Square) vs. the number of clusters as shown in Figure 10 to analyze the time series data of HVAC setpoints (actions) collected from human H_1 with over 100 simulated days. Figure 10 reveals that six clusters emerge as the predominant outcome for clustering numbers, aligning with the actual number of human activities in the simulation model.

Consequently, we compare the actual behavior of an individual (H_1) in the simulation model and the clustering results obtained by an eavesdropper (with six clusters) for each day. This comparison is presented in the top and middle subfigures of Figure 6. Figure 6 (middle) shows that the clustering is closely related to human activity patterns. In this scenario, the observer achieves an 87% accuracy in clustering. This indicates that after approximately 15 days (as seen in Figure 6), there are some discernible leaks of information regarding the human’s behavioral patterns. It’s important to note that the observer does not precisely infer the exact human activities. Nevertheless, we demonstrate here that the observer can deduce specific behavioral patterns of the human, leveraging their knowledge of the application domain. This allows them to make educated inferences, such as when the individual is likely to go to sleep, when they depart from their residence, or when there are deviations from the typical daily behavior of the individual.

6.3.3 PAPER-HILT Personalized Privacy-aware Adaptation. We evaluate the effectiveness of PAPER-HILT in adaptively reducing privacy vulnerabilities tied to human behavior while considering the privacy-utility tradeoff. To this end, we first start **PHASE 2** of the DQN training for PCL and UCL paths as described in algorithm 1. For **PHASE 2**, we interact with the environment to create utility and privacy buffers for specific values of privacy budget p and utility budget u as explained in sections 5.2.1 and 5.2.2. For instance, we assess the performance at $u = 0.85$ as shown in Table 1 for humans H_1 , H_2 , and H_3 . For H_1 with a utility budget of $u = 0.85$, exit branch 6 (L_6) has label 1 (satisfying the utility requirements) and is permitted during the inference, meaning that the network can choose this exit to meet the utility budget constraint ($u = 0.85$). After these interactions with the environment used to generate utility and privacy buffers, we start the **PHASE 2** training for UCL and PCL paths.

We implemented the **PHASE 2** training based on different budgets for privacy p and utility u to investigate the impact of those budgets on the permitted exit branches for different humans. Table 2 presents various values of u and p and allowed exit branches for each human. For instance, at $u = 0.75$ and $p = 0.7$, the allowed exit branches for H_1 are exits at layers L_1 and L_6 . Decreasing the

u	u = 0.95			u = 0.85			u = 0.75			u = 0.65			u = 0.55		
human	H ₁	H ₂	H ₃	H ₁	H ₂	H ₃	H ₁	H ₂	H ₃	H ₁	H ₂	H ₃	H ₁	H ₂	H ₃
p = 0.9	×	×	×	×	×	×	×	×	×	×	×	L ₃	L _{4,6}	L ₈	L _{2,3}
p = 0.8	×	×	×	×	×	×	L ₆	×	L ₃	L _{1,6}	L _{5,8}	L _{3,9}	L _{1,3,6}	L _{5,8}	L _{3,9}
p = 0.7	×	×	×	×	×	×	L _{1,6}	L ₈	L _{3,5}	L _{1,4,6}	L _{3,6,9}	L _{4,7}	L _{1,6}	L _{3,6,8}	L _{3,5,7}
p = 0.6	×	×	×	×	×	×	L _{1,6,7}	L _{5,8}	L _{3,4,5}	L _{1,6,7}	L _{5,8}	L _{3,4,5}	L _{1,6,7}	L _{4,5,7}	L _{4,7,8,9}

Table 2. PCL and UCL confidence per layer for all humans at various values of u and p .Fig. 11. Privacy-utility trade-off for three humans with various values of u .Fig. 12. Human behavior changes over time and the corresponding MI using $u = 0.75$ and $p = 0.7$.

values of the budgets is associated with a higher number of permitted exit branches. For instance, at $u = 0.75$ and $p = 0.6$, exits at layers L_1 , L_6 , and L_7 are permitted to take. We validated these outcomes by examining the eavesdropper’s ability to cluster the time series of shared actions with the cloud engine. We chose the first available branch among the permitted exit branches, but as they are labeled as “1,” they provide the same performance on utility and privacy. Figure 6 depicts the ground truth of the activities for human H_1 (top), the clustering result by the eavesdropper (middle) when there is no privacy mitigation, and the bottom one is clustering results after taking allowed exits (in this case exit layer L_6 with $u = 0.75$ and $p = 0.7$). As Figure 6 illustrates, the clustering capability of the eavesdropper drops to 61% accuracy after applying the mitigation, indicating an improvement in the privacy protection by 26% for human H_1 . We observed similar results for H_2 and H_3 with 23% and 21% improvement, respectively.

The effect of this using $u = 0.75$ and $p = 0.7$ on human H_1 is shown in Figure 8. The histogram of the PMV before and after using the PAPER-HILT shows that before mitigation (early exit at the optimal utility at Layer L_4), the percentage of PMV samples within the $[-0.5 - 0.5]$ is 86%, compared to 79% when using mitigation indicating a reduction in the performance by 9%. We have observed similar results for H_x and H_x with reduction performance of 12% and 16%, respectively.

6.3.4 PAPER-HILT Privacy-utility Tradeoff Analysis. We used the standard deviation (STD) of the PMV as a utility variation metric. A higher STD in PMV values signifies lower utility (indicating a broader spread of PMV values). We assessed the clustering accuracy as an indicator of privacy leakage against the STD of the PMV for various values of u . Figure 11 shows the privacy vs. utility plots using different values of u for all human subjects. Increasing the value of u corresponds to a decrease in the STD of the PMV, indicating better performance at the expense of lower privacy protection (higher clustering accuracy). On average, for all humans, utility (performance) drops by 23%, and privacy (state prediction) improves by 34%.

6.3.5 Adapting to Human Variability. During the inference, we monitor the current value of mutual information $I_{current}$ of the exit branch. If the $I_{current}$ drops below a certain percentage of the I_{max} – where I_{max} is the maximum of the I during the training PHASE 1, we retrain the Q network to adapt to this variability in human behavior. Figure 12 illustrates the MI for H_3 where the model learns the behavior MI adapts to that specific behavior. However, the human behavioral pattern eventually shifts to a new pattern, and MI begins to drop. After it drops below a certain threshold $I_{threshold} = 0.8$, the Q network is retrained and replaced by the new model. We observe the growth of the MI until it converges to a new maximum value to conform to the new behavior. To simulate this transition in behavior, we switched between the behaviors of H_3 and H_1 where the H_3 interacts with the environment for 25 days, and then we switched to H_1 for another 25 days of the simulation. It took 10 days to retrain the model and adapt to the new behavior. As depicted in Figure 12, this results in a newly adjusted MI curve that accommodates these alterations in human behavioral patterns.



Fig. 13. EMOTIV *EPOC_x* and Oculus device worn by a participant.

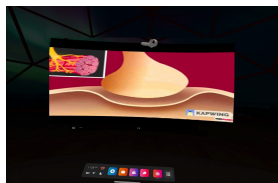


Fig. 14. Screenshot of the view of the Oculus device.

AL	1	1	1	1	0	0	0	0
FL	1	1	0	0	1	1	0	0
VL	1	0	1	0	1	0	1	0
State	S8	S7	S6	S5	S4	S3	S2	S1

Table 3. Human state is one of 8 states depending on the alertness level (AL), fatigue level (FL), and vertigo level (VL).

7 APPLICATION 2 - SMART CLASSROOM WITH VR TECHNOLOGY

In this section, we create a real-world virtual reality (VR) application to assess the effectiveness of PAPER-HILT. This decision was inspired by the recent transformation in the education sector, emphasizing personalized and remote learning setups. In prolonged training or educational sessions, especially in the online or remote context, human performance often deteriorates due to distractions, drowsiness, and fatigue [53]. In our experiment, we employ an RL agent to monitor these changes in the human state and offer personalized feedback to enhance learning performance. This RL agent operates from the cloud and has access to the actions executed by the RL model. As established in our previous experiment, these adaptive actions are linked to the individual’s private state, encompassing learning performance and mental well-being. Our approach commences with the design of the application, followed by the exploration of the relationship between the actions taken by the RL agent and the mental state of the human participant. Finally, we introduce the use of PAPER-HILT, to counteract potential breaches of private data.

7.1 System Design

We introduced two presentation modes, 2D and 3D, to deliver educational content to our study participants. To implement the 3D presentation, we harnessed cutting-edge Virtual Reality (VR) technologies, specifically utilizing an Oculus device. The choice of VR was informed by recent research, indicating its substantial potential for revolutionizing learning and workforce training [26]. Meanwhile, for the 2D presentation mode, we relied on traditional laptop screens. The content we used for these presentations was sourced from Khan Academy, along with its accompanying quizzes covering topics in biology [30], chemistry [32], and physics [31]. We engaged 15 participants, all within the age range of 20 to 30 years, to view these stand-alone lectures. Importantly, these lectures were designed to be comprehensible without any prerequisite knowledge on the participants’ part.

The primary task assigned to the participants was to attentively watch the lectures and subsequently respond to questions related to the content at the end. To facilitate the 3D experience, we transformed these 2D lectures into 3D versions suitable for VR presentations. Each lecture lasted 55 minutes and followed a narrative style, devoid of quizzes or interruptions. To gauge the mental states associated with learning, we equipped participants with EEG wearable devices. While various wearable devices are capable of measuring different physiological signals indicative of mental states (i.e., alertness or drowsiness), we opted for the EEG signal. This choice was based on recent research demonstrating that the activation of the frontal lobe in the brain can be leveraged to gauge an individual’s learning ability and cognitive performance [16]. We specifically employed the EMOTIV EPOC_X 14-channel portable EEG device [14]. Before the experiment, we administered a 10-minute 2D video presentation on a laptop screen to establish a baseline for participants’ mental state signals. In monitoring the participants’ alertness and readiness to learn, we analyzed the raw EEG data in 10-minute intervals. Each lecture was divided into 10-minute segments, referred to as “stages,” with approximately five such stages in each lecture⁵. Figure 13 illustrates the setup worn by a participant (VR and EEG). The laptop on the left casts the participant’s view on the Oculus device, and the laptop on the right presents the live EEG signal collected from the EMOTIV device. Figure 14 presents the screenshot of the view of the participant while watching biology content on an Oculus device with an office background.

7.2 RL Design

Although VR technologies have shown their advantages in both education and workplace training, people’s responses to VR environments can vary significantly. Some individuals may experience symptoms of vertigo and cybersickness while using VR, which can negatively impact the learning experience. To address this issue, we have defined the human state as a combination of

⁵The average attention span of the human is 10 to 15 minutes [38].

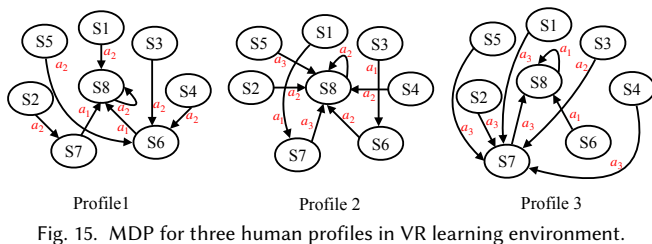


Fig. 15. MDP for three human profiles in VR learning environment.

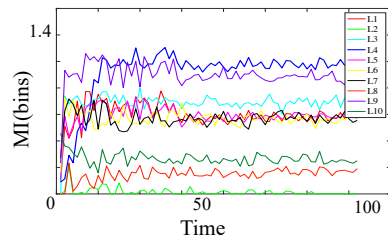


Fig. 16. Mutual information for all of the exit branches of profile 1.

three key features: alertness level (AL), fatigue level (FL), and vertigo level (VL). We have categorized these three features into binary classes to simplify our state space. Specifically, AL is classified as either “Alert (1)” or “Not Alert (0),” FL is categorized as “Fatigue (1)” or “Vigor (0),” and VL is grouped as “Not Vertigo (1)” or “Hypocalcemia (0).” We represent the human state as a tuple of these three features: $S = \{(AL, FL, VL) : AL \in \{0, 1\}, FL \in \{0, 1\}, VL \in \{0, 1\}\}$. Table 3 depicts an overview of the state space.

Each feature is determined based on a specific threshold (δ_{AL} , δ_{FL} , δ_{VL}). If a feature’s measured value surpasses the threshold, it is categorized as 1; otherwise, it is labeled as 0. The optimal human state for effective learning is s_8 , where the individual is alert and not experiencing cybersickness (neither fatigue nor vertigo). Conversely, the least favorable state is s_1 , where the person is not alert and suffers from cybersickness (both fatigue and vertigo). It’s important to note that individuals can transition between these states, and these threshold values can be adjusted to suit the specific application and participants. To determine the human state (AL, FL, VL) and compute the thresholds (δ_{AL} , δ_{FL} , δ_{VL}) we follow the procedure studied in [50].

The action space \mathcal{A} in our VR application includes the following actions: (1) Giving a break to the user, (2) Enabling VR mode by transitioning from 2D to 3D, (3) Disabling VR mode by reverting from 3D to 2D, (4) Altering the content of the presentation, and (5) Maintaining the state in the learning environment (no change). Notably, activating VR mode heightens cognitive engagement and improves learning performance. However, some users may encounter cybersickness when exposed to VR, necessitating the reinforcement learning agent to revert to the standard 2D mode to alleviate cybersickness symptoms. Additionally, taking a break during a learning session may also be necessary to combat drowsiness, cybersickness symptoms, or cognitive overload. Therefore, \mathcal{A} is a finite and bounded set of discrete actions within the range of $[1, 5]$: $\mathcal{A} = \{a : a \in [1, 5], a \in \mathbb{N}\}$. The performance of individuals in a quiz determines the reward value assigned after each learning module. The score in this quiz is expressed as a percentage. The quantification of the quiz is based on ten multiple-choice questions, with perfect and zero scores corresponding to 10/10 (100%) and 0/10 (0%), and scores receive rewards 100 and 0, respectively.

7.3 PAPER-HILT Adaptation

We designed the same *DQN* network described in section 6.3.1. Accordingly, we employed the dataset of 15 participants to classify their behaviors into three distinct groups. The initial group comprises individuals highly tolerant to VR, indicating they do not encounter simulator sickness even after prolonged use of VR devices exceeding 20 minutes. The second group includes individuals who may exhibit cybersickness during VR exposure, while the third group consists of individuals with the lowest VR tolerance. We represent the behavior of these groups using Markov Decision Processes (MDP), as illustrated in Figure 15 as described in [58]. Subsequently, we started **PHASE 1** in PAPER-HILT, which has “sequential training” with up to 10 layers. We trained three independent *DQNs* for the three profiles. Figure 16 illustrates the mutual information for all branches of the *DQN* trained for profile1. As Figure 16 depicts, exit branch L_4 of profile 1 has the highest mutual information growth.

7.4 Privacy Leak

As in our outlined threat model, eavesdroppers within the cloud environment can access RL actions and utilize machine learning algorithms to infer confidential information related to participants. The calculation of the human state occurs at the edge, and the privacy of the human mental state is of utmost significance. Any unauthorized access to this information by potential attackers is regarded as a breach of privacy. The prediction of the human state is utilized, and we gauge the accuracy of human state prediction through clustering, similar to application 1, to measure privacy leaks. It is important to highlight that even if the eavesdropper is

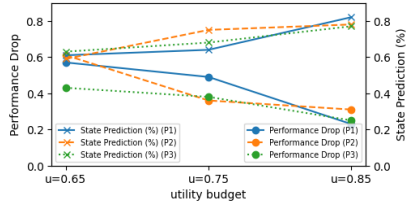


Fig. 17. Privacy-utility trade-off for three profiles with various values of u .

u	$u = 0.85$			$u = 0.75$			$u = 0.65$			$u = 0.55$		
human	P_1	P_2	P_3	P_1	P_2	P_3	P_1	P_2	P_3	P_1	P_2	P_3
$p = 0.9$	×	×	×	×	×	×	×	×	×	×	×	×
$p = 0.8$	×	×	×	L_4	L_5	L_7	$L_{2,4}$	$L_{5,7}$	$L_{6,7}$	$L_{2,4,8}$	$L_{1,5,8}$	$L_{7,8}$
$p = 0.7$	×	×	×	$L_{3,4,6}$	$L_{5,9}$	$L_{3,5,6}$	$L_{4,7}$	$L_{4,5,9}$	$L_{4,7}$	$L_{1,6}$	$L_{3,6,8}$	$L_{3,5,7}$
$p = 0.6$	×	×	L_3	$L_{1,6,7}$	$L_{4,5}$	$L_{4,5,9}$	$L_{2,4,10}$	$L_{5,8,9}$	$L_{4,7}$	$L_{1,4,9}$	$L_{4,5,7}$	$L_{7,8,10}$

Table 4. *PCL* and *UCL* confidence per layer for all profiles at various values of utility budget u and privacy budget p .

unaware of the exact human state, the alteration in the human state (learning pattern) resulting from observed actions can be deduced, potentially revealing private information such as the human attention span.

Figure 16 visually represents the mutual information growth between actions taken by the human profile 1 and the states of the associated profile, where the mutual information of exit branch L_4 is observed to reach approximately 1.3 bits. A strategy similar to the one devised for eavesdropping in our initial application can also be applied to this scenario. Eavesdroppers can employ unsupervised learning methods, such as clustering, where our analysis shows that it can reach 82% of accuracy for profile 1.

7.5 PAPER-HILT Personalized Privacy-aware Adaptation

We evaluate the PAPER-HILT’s effectiveness in adaptively reducing privacy vulnerabilities, considering the privacy-utility tradeoff. This involves initiating the second phase of *DQN* training for *PCL* and *UCL* paths, as specified in algorithm 1. For **PHASE 2** training, we follow the same steps described in section 6.3.3. Table 4 depicts the different budgets of u and p and the permitted exit branches for each profile. For instance, at $u = 0.75$ and $p = 0.7$, the allowed exit branches for P_1 are exits at layers L_3 , L_4 and L_6 . Furthermore, we evaluate the trade-off between utility (drop in performance) and the amount of the data leak (state prediction) as illustrated in Figure 17. For instance, for P_1 at utility budget $u = 0.75$, the state prediction accuracy is 75%. On average, for all profiles, utility (performance) drops by 28%, and privacy (state prediction) improves by 28%.

8 CONCLUSION

In this paper, we introduced PAPER-HILT, an innovative approach that combines the strengths of adaptive personalized DRL with an early-exit strategy. This early-exit mechanism is a critical addition, allowing the system to make prompt and informed decisions during the learning process. It enables the system to efficiently navigate the complexities of privacy concerns, swiftly intervening when privacy risks are detected. This approach is particularly beneficial in scenarios where user behavior varies, catering to the individualized nature of privacy requirements. By integrating this early-exit strategy into the DRL framework, PAPER-HILT offers an effective solution for managing the privacy-utility tradeoff, tailored to the specific needs and variations in human behavior within HITL IoT environments. On average, across two HITL applications, PAPER-HILT is able to mitigate privacy leaks by 31% while still providing acceptable utility.

Through PAPER-HILT, we aim to set a new standard in the development of privacy-aware IoT systems, emphasizing the importance of responsive and adaptable AI techniques in addressing the evolving landscape of privacy concerns in technology, especially with human behavioral variability.

9 ACKNOWLEDGMENTS

This research was partially supported by the National Science Foundation (NSF) awards 2105084 and 2339266. The authors would like to thank the Center for Embedded & Cyber-physical Systems (CECS) at UCI for partially supporting Mojtaba Taherisadr with the 2023-2024 ECPS Fellowship during the development of this work.

REFERENCES

- [1] Armand Ahadi-Sarkani and Salma Elmalaki. 2021. Adas-rl: Adaptive vector scaling reinforcement learning for human-in-the-loop lane departure warning. In *Proceedings of the First International Workshop on Cyber-Physical-Human System Design and Implementation*. 13–18.
- [2] ASHRAE/ANSI Standard 55-2010 American Society of Heating, Refrigerating, and Air-Conditioning Engineers. 2010. Thermal environmental conditions for human occupancy. *Inc. Atlanta, GA, USA* (2010).
- [3] Judith Barrett, Leon Lack, and Mary Morris. 1993. The sleep-evoked decrease of body temperature. *Sleep* 16, 2 (1993), 93–99.
- [4] Lauren Bass. 2019. The Concealed Cost of Convenience: Protecting Personal Data Privacy in the Age of Alexa. *Fordham Intell. Prop. Media & Ent. LJ* 30 (2019), 261.

- [5] Phuthipong Bovornkeeratiroj, Srinivasan Iyengar, Stephen Lee, David Irwin, and Prashant Shenoy. 2020. Repel: A utility-preserving privacy system for iot-based energy meters. In *2020 IEEE/ACM Fifth International Conference on Internet-of-Things Design and Implementation (IoTDI)*. IEEE, 79–91.
- [6] Kelly Caine. 2009. *Exploring everyday privacy behaviors and disclosures*. Georgia Institute of Technology.
- [7] João Miguel Reis Araújo Proença Cambeiro. 2019. *The Human in the loop in Cyber-Physical Systems: the case of Building Automation*. Ph.D. Dissertation.
- [8] campbellsci. 2022. black globe thermometer. Retrieved June 10, 2022 from <https://www.campbellsci.com/blackglobe>
- [9] Robert G Carroll. 2006. *Elsevier's Integrated Physiology E-Book*. Elsevier Health Sciences.
- [10] Wuhui Chen, Xiaoyu Qiu, Ting Cai, Hong-Ning Dai, Zibin Zheng, and Yan Zhang. 2021. Deep reinforcement learning for Internet of Things: A comprehensive survey. *IEEE Communications Surveys & Tutorials* 23, 3 (2021), 1659–1692.
- [11] Salma Elmalaki. 2021. Fair-iot: Fairness-aware human-in-the-loop reinforcement learning for harnessing human variability in personalized iot. In *Proceedings of the International Conference on Internet-of-Things Design and Implementation*. 119–132.
- [12] Salma Elmalaki, Yasser Shoukry, and Mani Srivastava. 2018. Internet of Personalized and Autonomous Things (IoPAT): Smart Homes Case Study. In *Proceedings of the 1st ACM International Workshop on Smart Cities and Fog Computing*. ACM, 35–40.
- [13] Salma Elmalaki, Huey-Ru Tsai, and Mani Srivastava. 2018. Sentio: Driver-in-the-loop forward collision warning using multisample reinforcement learning. In *Proceedings of the 16th ACM Conference on Embedded Networked Sensor Systems*. 28–40.
- [14] EMOTIV. 2020. EMOTIV EPOC+ 14 Channel Mobile Brainwear. <https://www.emotiv.com/product/emotiv-epoc-14-channel-mobile-eeg/>. Last accessed June 2023.
- [15] Ecenaz Erdemir, Pier Luigi Dragotti, and Deniz Gündüz. 2020. Privacy-Aware Time-Series Data Sharing With Deep Reinforcement Learning. *IEEE Transactions on Information Forensics and Security* 16 (2020), 389–401.
- [16] Paul J Eslinger and Antonio R Damasio. 1985. Severe disturbance of higher cognition after bilateral frontal lobe ablation: patient EVR. *Neurology* 35, 12 (1985), 1731–1731.
- [17] Poul O Fanger. 1970. Thermal comfort. Analysis and applications in environmental engineering. *Thermal comfort. Analysis and applications in environmental engineering*. (1970).
- [18] Aviezi S Fraenkel. 2004. Complexity, appeal and challenges of combinatorial games. *Theoretical Computer Science* 313, 3 (2004), 393–415.
- [19] Evrard Garcelon, Kamalika Chaudhuri, Vianney Perchet, and Matteo Pirota. 2022. Privacy amplification via shuffling for linear contextual bandits. In *International Conference on Algorithmic Learning Theory*. PMLR, 381–407.
- [20] Evrard Garcelon, Vianney Perchet, Ciara Pike-Burke, and Matteo Pirota. 2021. Local differential privacy for regret minimization in reinforcement learning. *Advances in Neural Information Processing Systems* 34 (2021), 10561–10573.
- [21] Michael Gerber. 2014. energyplus energy Simulation Software. (2014).
- [22] Dylan Hadfield-Menell, Stuart J Russell, Pieter Abbeel, and Anca Dragan. 2016. Cooperative inverse reinforcement learning. *Advances in neural information processing systems* 29 (2016).
- [23] Alexander Hans, Daniel Schneegaß, Anton Maximilian Schäfer, and Steffen Udluft. 2008. Safe exploration for reinforcement learning.. In *ESANN*. 143–148.
- [24] Jakub P Hlávka. 2020. Security, privacy, and information-sharing aspects of healthcare artificial intelligence. In *Artificial Intelligence in Healthcare*. Elsevier, 235–270.
- [25] Junyuan Hong, Zhangyang Wang, and Jiayu Zhou. 2022. Dynamic privacy budget allocation improves data efficiency of differentially private gradient descent. In *Proceedings of the 2022 ACM Conference on Fairness, Accountability, and Transparency*. 11–35.
- [26] María Blanca Ibáñez, Ángela Di Serio, Diego Villarán, and Carlos Delgado Kloos. 2014. Experimenting with electromagnetism using augmented reality: Impact on flow student experience and educational effectiveness. *Computers & Education* 71 (2014), 1–13.
- [27] T Io. 2011. economic and Business Dimensions online advertising, Behavioral targeting, and Privacy. *Communications of the ACM* 54, 5 (2011).
- [28] Richeng Jin, Xiaofan He, and Huaiyu Dai. 2017. On the tradeoff between privacy and utility in collaborative intrusion detection systems—a game theoretical approach. In *Proceedings of the Hot Topics in Science of Security: Symposium and Bootcamp*. 45–51.
- [29] Wooyoung Jung and Farrokh Jazizadeh. 2017. Towards integration of doppler radar sensors into personalized thermoregulation-based control of HVAC. In *Proceedings of the 4th ACM International Conference on Systems for Energy-Efficient Built Environments*. ACM, 21.
- [30] KhanAcademy. 2021. AP College Biology. <https://www.khanacademy.org/science/ap-biology>. Accessed: 2021-10-07.
- [31] KhanAcademy. 2021. AP College Physics. <https://www.khanacademy.org/science/ap-physics-2>. Accessed: 2021-10-07.
- [32] KhanAcademy. 2021. Organic Chemistry. <https://www.khanacademy.org/science/organic-chemistry>. Accessed: 2021-10-07.
- [33] Adarsh Kumar Kosta, Malik Aqeel Anwar, Priyadarshini Panda, Arijit Raychowdhury, and Kaushik Roy. 2022. RAPID-RL: A Reconfigurable Architecture with Preemptive-Exits for Efficient Deep-Reinforcement Learning. In *2022 International Conference on Robotics and Automation (ICRA)*. IEEE, 7492–7498.
- [34] Chin Leong Lim, Chris Byrne, and Jason KW Lee. 2008. Human thermoregulation and measurement of body temperature in exercise and clinical settings. *Annals Academy of Medicine Singapore* 37, 4 (2008), 347.
- [35] Mohammad Malekzadeh, Dimitrios Athanasakis, Hamed Haddadi, and Ben Livshits. 2020. Privacy-preserving bandits. *Proceedings of Machine Learning and Systems* 2 (2020), 350–362.
- [36] MATLAB. 2022. Thermal Model of a House. Retrieved June 10, 2022 from <https://www.mathworks.com/help/simulink/slref/thermal-model-of-a-house.html>
- [37] Yoshitomo Matsubara, Marco Levorato, and Francesco Restuccia. 2022. Split computing and early exiting for deep learning applications: Survey and research challenges. *Comput. Surveys* 55, 5 (2022), 1–30.
- [38] W. J. McKeachie and M. Svinicki. 2006. *McKeachie's teaching tips: Strategies, research, and theory for college and university teachers (12th ed.)*. Houghton-Mifflin.
- [39] Shilpi Mishra, Divyapratap Singh, Divyansh Pant, and Akash Rawat. 2022. Secure Data Communication Using Information Hiding and Encryption Algorithms. In *2022 Second International Conference on Artificial Intelligence and Smart Energy (ICAIS)*. IEEE, 1448–1452.
- [40] Anh Nguyen, Raghda Alqurashi, Zohreh Raghebi, Farnoush Banaei-Kashani, Ann C Halbower, and Tam Vu. 2016. A lightweight and inexpensive in-ear sensing system for automatic whole-night sleep stage monitoring. In *Proceedings of the 14th ACM Conference on Embedded Network Sensor Systems*. 230–244.
- [41] Berend Olivier, Theo Zethof, Tommy Pattij, Meg van Boogaert, Ruud van Oorschot, Christina Leahy, Ronald Oosting, Arjan Bouwknecht, Jan Veening, Jan van der Gugten, et al. 2003. Stress-induced hyperthermia and anxiety: pharmacological validation. *European journal of pharmacology* 463, 1-3 (2003), 117–132.
- [42] Liberty Adams Omonkhoa. 2021. A review of the issues and challenges in IoT security using machine learning techniques. (2021).
- [43] Xinlei Pan, Weiyao Wang, Xiaoshuai Zhang, Bo Li, Jinfeng Yi, and Dawn Song. 2019. How You Act Tells a Lot: Privacy-Leaking Attack on Deep Reinforcement Learning. *AAMAS* (2019).
- [44] Franz Papst, Naomi Stricker, Rahim Entezari, and Olga Saukh. 2022. To Share or Not to Share: On Location Privacy in IoT Sensor Data. In *2022 IEEE/ACM Seventh International Conference on Internet-of-Things Design and Implementation (IoTDI)*. IEEE, 128–140.

- [45] Neel Patel, Reza Shokri, and Yair Zick. 2022. Model explanations with differential privacy. In *Proceedings of the 2022 ACM Conference on Fairness, Accountability, and Transparency*. 1895–1904.
- [46] Maria Petrescu and Anjala S Krishen. 2018. Analyzing the analytics: data privacy concerns. , 41–43 pages.
- [47] Dorsa Sadigh, Anca D Dragan, Shankar Sastry, and Sanjit A Seshia. 2017. *Active preference-based learning of reward functions*.
- [48] Tal Shany, Stephen J Redmond, Michael R Narayanan, and Nigel H Lovell. 2012. Sensors-based wearable systems for monitoring of human movement and falls. *IEEE Sensors Journal* 12, 3 (2012), 658–670.
- [49] Sopicha Stirapongsasuti, Wataru Sasaki, and Keiichi Yasumoto. 2019. Decision making support for privacy data upload in smart home. In *Adjunct Proceedings of the 2019 ACM International Joint Conference on Pervasive and Ubiquitous Computing and Proceedings of the 2019 ACM International Symposium on Wearable Computers*. 214–217.
- [50] Mojtaba Taherisadr, Mohammad Abdullah Al Faruque, and Salma Elmalaki. 2023. Erudite: Human-in-the-loop iot for an adaptive personalized learning system. *IEEE Internet of Things Journal* (2023).
- [51] Mojtaba Taherisadr, Stelios Andrew Stavroulakis, and Salma Elmalaki. 2023. adaparl: Adaptive privacy-aware reinforcement learning for sequential-decision making human-in-the-loop systems. *arXiv preprint arXiv:2303.04257* (2023).
- [52] Surat Teerapittayanon, Bradley McDanel, and Hsiang-Tsung Kung. 2016. Branchynet: Fast inference via early exiting from deep neural networks. In *2016 23rd international conference on pattern recognition (ICPR)*. IEEE, 2464–2469.
- [53] Shogo Terai, Shizuka Shirai, Mehrasa Alizadeh, Ryosuke Kawamura, Noriko Takemura, Yuki Uranishi, Haruo Takemura, and Hajime Nagahara. 2020. Detecting Learner Drowsiness Based on Facial Expressions and Head Movements in Online Courses. In *Proceedings of the 25th International Conference on Intelligent User Interfaces Companion*. 124–125.
- [54] The New York Times. 2022. The Best Smart Thermostat. <https://www.nytimes.com/wirecutter/reviews/the-best-thermostat/>. Accessed: 2022-06-10.
- [55] Baoxiang Wang and Nidhi Hegde. 2019. Privacy-preserving q-learning with functional noise in continuous spaces. *Advances in Neural Information Processing Systems* 32 (2019).
- [56] Yashuo Wu, Carla Fabiana Chiasserini, Francesco Malandrino, and Marco Levorato. 2023. Enhancing Privacy in Federated Learning via Early Exit. In *Proceedings of the 5th workshop on Advanced tools, programming languages, and PLatforms for Implementing and Evaluating algorithms for Distributed systems*. 1–5.
- [57] Wanrong Zhang, Olga Ohrimenko, and Rachel Cummings. 2022. Attribute privacy: Framework and mechanisms. In *Proceedings of the 2022 ACM Conference on Fairness, Accountability, and Transparency*. 757–766.
- [58] Tianyu Zhao, Mojtaba Taherisadr, and Salma Elmalaki. 2023. FAIRO: Fairness-aware Adaptation in Sequential-Decision Making for Human-in-the-Loop Systems. *arXiv preprint arXiv:2307.05857* (2023).